Embedded-atom-method tantalum potential developed by the force-matching method

Youhong Li,[1] Donald J. Siegel,[2] James B. Adams,[1] and Xiang-Yang Liu[3]
[1]*Chemical and Materials Engineering Department, Arizona State University, Tempe, Arizona 85281-6006*
[2]*Sandia National Laboratories, Mail Stop 9161, Livermore, California 94551*
[3]*Computational Nanoscience Group, Physical Sciences Research Laboratories, Motorola Incorporated, Los Alamos, New Mexico 87544*
(Received 24 May 2002; revised manuscript received 9 September 2002; published 4 March 2003)

An embedded-atom-method potential for tantalum (Ta) has been carefully constructed by fitting to a combination of experimental and density-functional theory (DFT) data. The fitted data include the elastic constants, lattice constant, cohesive energy, unrelaxed vacancy formation energy, and hundreds of force data calculated by DFT for a variety of structures such as liquids, surfaces, clusters, interstitials, vacancies, and stacking faults. We also fit to the cohesive energy vs volume data from the equation of state for the body-centered-cubic (bcc) Ta and to the calculated cohesive energy using DFT for the face-centered-cubic (fcc) Ta structure. We assess the accuracy of the new potential by comparing several calculated Ta properties with those obtained from other potentials previously reported in the literature. In many cases, the new potential yields superior accuracy at a comparable or lower computational cost.

DOI: 10.1103/PhysRevB.67.125101 PACS number(s): 34.20.−b

I. INTRODUCTION

Tantalum (Ta) is used in a wide variety of applications ranging from microelectronics to nuclear power. It can form a stable oxide and is a promising diffusion barrier for copper (Cu) metallization in very large scale integrated applications[1–4] because Cu and Ta have very limited mutual solubility. Analysis of Cu-Ta castings prepared by adding Ta to molten Cu indicated a Ta-in-Cu solubility of 0.025 wt % (0.0088 at. %) at 1200 °C. Wong[5,6] *et al.* found that Cu films grow heteroepitaxially on tetragonal Ta films with the crystallographic orientation of $Cu_{(111)[220]}//Ta_{(002)[330]}$. The heteroepitaxial growth of Cu enhances the formation of large grains with a strong (111) texture, which is expected to improve the reliability of Cu interconnects. Sputtered Cu seed layers on Ta typically have a stronger (111) texture than on TiN.[5,6] With the advent of nanotechnology, atomic scale simulations of materials' behavior are becoming increasingly important. A reliable empirical Ta potential is important both for understanding the behavior of Ta in its pure form and for constructing reliable alloy potentials for application to systems such as Cu-Ta.

Empirical potentials for Ta have been proposed by several groups, including Finnis-Sinclair,[7] a Johnson-Oh embedded-atom-method (EAM),[8] a Guellil-Adams EAM,[9] a MEAM potential by Lee *et al.*,[10] a EAM potential based on quantum mechanical calculations (named qEAM) by Wang *et al.*,[11] a bond-order potential by Mrovec *et al.*,[12] and a model generalized pseudopotential theory (MGPT) potential by Moriarty *et al.*[13] An analytical EAM potential for Ta was constructed by Johnson and Oh,[8] which was slightly modified by Guellil and Adams and tested against properties such as the phonon spectrum[9] (the Guellil-Adams potential is basically the same as the Johnson-Oh potential except that some of the functions were slightly changed to improve their fit to the vacancy properties). However our recent test of the Guellil-Adams potentials revealed that the calculated bulk modulus underestimated experiment by 27%. The Finnis-Sinclair potential[7] has the same form as the EAM but is derived from a different physical basis. The original Finnis-Sinclair potential was improved later due to its unphysical behavior at small interatomic separation.[14,15] The qEAM is an EAM potential fit only to data from quantum-mechanical calculations.[16] The MEAM potential[10] adds an angular term to the original EAM functional form. The bond-order potential[12] also includes an angular term, which results in about two orders-of-magnitude more computational cost. The MGPT (Ref. 13) Ta potential includes angular and multi-ion potential terms that reflect the partially filled *d* bands, thus it is computationally more expensive.

In this paper, we focus on developing an EAM Ta potential which can be applied to calculating equilibrium as well as nonequilibrium properties for Ta. We make use of the force-matching method, which has previously been used to develop potentials for Al,[17] Mg,[18] Al-Mg,[19] Al-Cu,[20] and Al-Pb.[21] However, to ensure the reliability of our potential, we have introduced an improved fitting scheme, which will be discussed later. The remainder of this paper is organized as follows: in Sec. II, we introduce our methodology; in Sec. III, we assess the accuracy of our potential and make comparisons to other published potentials.

II. METHODOLOGY

The EAM was originally developed by Daw and Baskes[22] and has been widely used to calculate properties of various metallic materials. The functional form of the EAM potentials is given by

$$E_{\mathrm{tot}}=\frac{1}{2}\sum_{i\neq j} V(r_{ij})+\sum_{i} F(\rho_i), \tag{1}$$

$$\rho_i=\sum_{j} \phi(r_{ij}). \tag{2}$$

Here E_{tot} is the total energy, $V(r_{ij})$ is the pair potential, and $F(\rho)$ is the embedding function. $\phi(r_{ij})$ is the electron-density contribution from atom *j* to atom *i*. The total electron

density ρ_i at an atom position i is computed via a linear superposition of electron-density contributions from neighboring atoms.

Empirical potentials such as the EAM usually describe the atomic interactions by several analytical functions. Arbitrary assumptions as to the form of the functions are often made within the given analytical framework so as to reduce the number of parameters to a manageable level. These parameters are usually determined by fitting to a set of experimental data at 0 K, with most of the data being for perfect crystals such as lattice constant, cohesive energy, and elastic constants.

With the progress in computational methods based on density-functional theory (DFT),[23,24] it is possible to obtain atomic forces of high quality for a very large number of atomic configurations, including different geometries such as defects, clusters, molecules, and liquids. However, these methods are computationally much more expensive, and are therefore limited to small systems (hundreds of atoms) for short times (pico seconds).

When constructing an empirical potential, it is beneficial to include first-principles force data in addition to experimental data because it provides for a more accurate and transferable potential. To these ends, the force-matching method was developed by Ercolessi and Adams[17] to obtain realistic empirical potentials by making use of very large amounts of information obtained by first-principles calculations. The numerical engine is based on trying to reproduce the first-principles forces and the experimental data with those calculated by the potential. The optimization is performed by carrying out a multidimensional minimization in a relatively large parameter space (of the order of 60 parameters). By explicitly including different atomic geometries and different temperatures, one can construct a potential that fits DFT forces at different geometries and temperatures, thus improving the transferability of empirical potentials. Indeed, potentials constructed with the force-matching method have been used extensively and with much success in predicting materials properties.[25–34] A similar approach was also adopted by Mishin *et al.*[35] for Al, Ni, and Ni-Al alloys.

In this work, we use the force-matching method to develop an EAM potential for Ta. The fitted experimental data and other material parameters from DFT calculations include lattice constant, cohesive energy, unrelaxed vacancy formation energy, bulk modulus, and elastic constants C_{11}, C_{12}, and C_{44}.

For the force database, initial atomic structures were created and short molecular-dynamics (MD) simulations were performed to equilibrate each structure for different temperatures. In these MD simulations, we used the Guellil-Adams[9] analytical Ta potential. After equilibration, we extracted a small part of the original cell and adjusted the boundary conditions to ensure that no atoms are within 2.39 Å (except for the structure that contains an interstitial). This is a simple, approximate method to obtain a reasonable set of structures. The structures are not true equilibrium structures, but are quite adequate for providing a wide range of forces. The structures are listed in Table I.

TABLE I. Structures for force calculation.

Structure Number	Structure name	Number of atoms[a]
1	BCC Ta, ~2500 K	16
2	BCC Ta, ~500 K	16
3	β-Ta, ~1000 K	30
4	β-Ta, ~2000 K	30
5	β-Ta surface at 500 K with adatoms	31
6	β-Ta surface at 500 K with more adatoms	32
7	BCC Ta, stacking fault	32
8	BCC Ta, ~1500 K, one vacancy	15
9	Ta cluster, ~500 K	10
10	Liquid Ta, ~4500 K	19
11	BCC Ta one interstitial, 1500 K	17

[a]This refers to the number of atoms in each structure used for DFT force calculations.

Our first-principles force database was calculated with the Vienna *ab initio* simulation package (VASP),[36] a DFT code based on projector augmented-wave pseudopotentials[37,38] and a plane-wave basis set. We chose the generalized-gradient approximation exchange-correlation functional of Perdew *et al.*[39] since it more accurately reproduces many experimental bulk properties (bulk modulus and equilibrium lattice constant) in comparison to the local-density approximation (LDA).[24] To ensure a high degree of precision, the Ta $5p$ and $6s$ semicore states were treated explicitly as the valence in the pseudopotential. Convergence testing on a bulk structure revealed that a plane-wave cutoff energy of 280 eV was sufficient to converge the total energy to within 1 meV/atom. Since the convergence of atomic forces is generally slower than that for energies, we used dense samplings of k space to obtain precise forces: up to 256 Monkhorst-Pack[40] k points were necessary to converge forces to within about ~5 meV/Å.

In addition, we also include energy data from the Rose *et al.* equation of state[41] of bcc Ta for various contractions and expansions of the unit cell as shown in Table II. These values would be very similar (within 0.85 eV) to our DFT data if they were slightly rescaled to the experimental bulk modulus, cohesive energy, and lattice constant.

In the fitting process, an objective function $Z(\langle\alpha\rangle)$ is constructed and minimized. This function has three parts as follows,

TABLE II. Energy from Rose *et al.* (Ref. 40) equation of state for the potential fit.

a/a_0	0.90	0.94	0.97	1.05	1.11	1.20	1.30
Rose *et al.* energy (eV)	−6.636	−7.643	−7.990	−7.885	−7.291	−6.139	−4.869

$$Z(\langle\alpha\rangle)=Z_{\text{forces}}(\langle\alpha\rangle)+Z_{\text{experi}}(\langle\alpha\rangle)+Z_w(\langle\alpha\rangle), \quad (3)$$

with

$$Z_{\text{forces}}(\langle\alpha\rangle)=\left(3\sum_{k=1}^{M}N_k\right)^{-1}\sum_{k=1}^{M}\sum_{i=1}^{N_k}[F_{ki}(\langle\alpha\rangle)-F_{ki}^0]^2, \quad (4)$$

$$Z_{\text{experi}}(\langle\alpha\rangle)=\sum_{l=1}^{P}W_l[A_l(\langle\alpha\rangle)-A_l^0]^2, \quad (5)$$

$$Z_w(\langle\alpha\rangle)=\sum_{k=1}^{f}\sum_{j=2}^{M_k}W_{kj}|\Delta J_{kj}|. \quad (6)$$

This first part $Z_{\text{forces}}(\langle\alpha\rangle)$ is from the difference between DFT forces and predicted forces by the fitted potential; the second part $Z_{\text{experi}}(\langle\alpha\rangle)$ is from the difference between material parameters and those predicted by the fitted potential. $F_{ki}(\langle\alpha\rangle)$ is the predicted force by the potential for the ith atom in the kth structure; F_{ki}^0 is the corresponding DFT force for the ith atom in the kth structure. N_k is the number of atoms in the kth structure. M is the total number of structures used for the fitting. $A_l(\langle\alpha\rangle)$ is the lth material parameter predicted by the fitted potential; A_l^0 is the corresponding material parameter. W_l is an assigned weight to the lth parameter used in the fitting. P is the total number of material parameters we fitted to. One can find more information on these two parts of the objective function from Ref. 17. $Z_w(\langle\alpha\rangle)$ is a term whose purpose is to minimize arbitrary fluctuations in the potential function. $\Delta J_{j'j}$ is defined as follows,

$$\Delta J_{j'j}=J_j-J_{j'}, \quad (7)$$

where J_j and $J_{j'}$ are function values at point j and its adjacent point j', respectively, where arbitrary fluctuation appears. W_{kj} is the fitting weight for the arbitrary variations. The f in the $Z_w(\langle\alpha\rangle)$ term is the number of functions we have in the potential. In this work $f=3$ since we have three functions, namely, electron density, pair potential, and embedding function. M_k is the number of points in function k. In our fitting, the downhill simplex method was used because it is efficient and robust.

In the EAM, potential functions for pure elements are invariant under the transformations (i) $\phi(R)\rightarrow A\phi(R)$, $F(\rho)\rightarrow F(\rho/A)$ and (ii) $V(r)\rightarrow V(r)+2B\rho(r)$, $F(\rho)\rightarrow F(\rho)-B\rho$. The two constants A and B are arbitrary and must be fixed by the external conditions. We choose $\rho_{\text{bulk}}=1$ and $F'(\rho_{\text{bulk}})=0$ to fix A and B. The ρ_{bulk} is the background electron density around an atom in a perfect crystal at equilibrium.

Each function is expressed with cubic splines. We believe that it is more flexible to express each potential function in cubic splines than to express it in only one analytic form within the simple EAM model. In other words, cubic splines with their piecewise parts, each of which having its own coefficients, could describe materials properties better than a single analytical function. In our fitting with cubic splines, natural boundary conditions were imposed and the first two derivatives at the common point of two neighboring cubic splines were continuous. For each function, we chose 23 parameters, with a cutoff value of 3.987 Å for both electron density and pair potential. This distance is halfway between the second- and third-nearest-neighbor distances and is reasonable for bcc metals, for which the second-nearest neighbors must be considered due to their nonclosely packed structure.

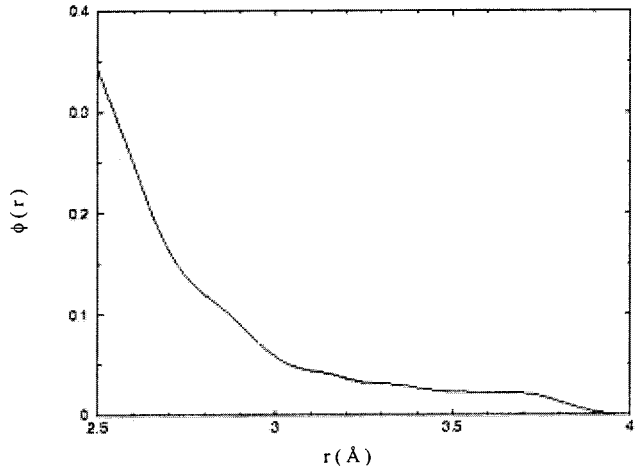

FIG. 1. Electron density $\phi(r)$ as a function of distance r from the center of an atom.

III. RESULTS AND DISCUSSION

The final fitting result for each function $\phi(r)$, $F(\rho)$, and $V(r)$ is shown in Figs. 1–3, respectively. $F'(\rho_{\text{bulk}})=0$ at $\rho_{\text{bulk}}=1$ can be seen from Fig. 2 since we applied the invariance properties. Ta properties calculated with the new potential are compared with experimental and DFT data in Table III, where it can be seen that very good agreement is obtained, especially for the bulk modulus with a reduction of error from 27% to about 8%, compared to the analytical Ta potential.[9] The lattice constant and cohesive energy are exactly the same as the experimental data.

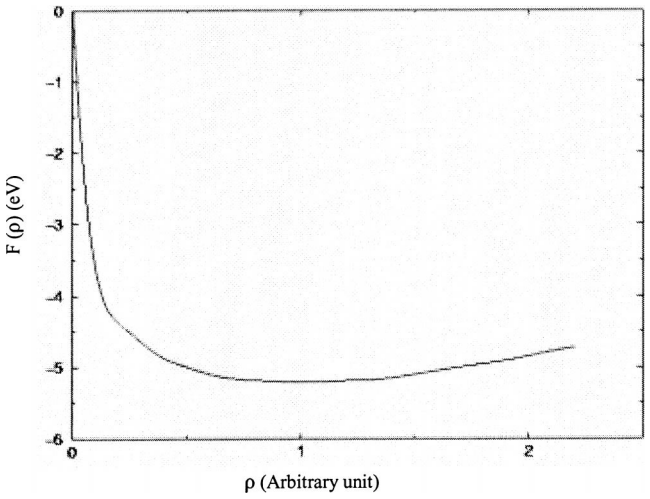

FIG. 2. Embedding function $F(\rho)$ as a function of the local electron density ρ.

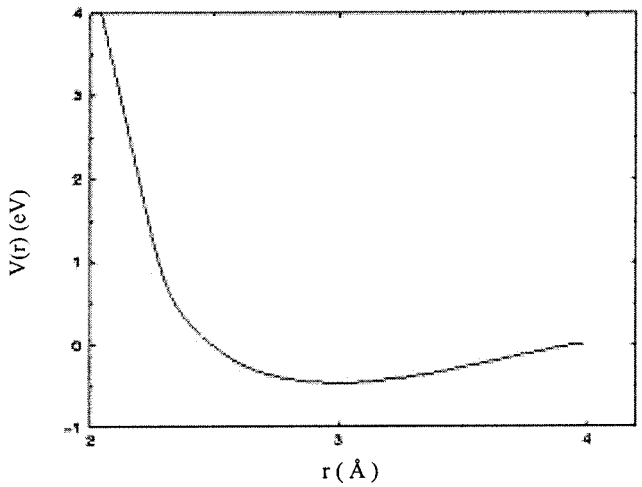

FIG. 3. Pair potential $V(r)$ as a function of the distance r between a pair of atoms.

The error in fitting to DFT forces is on average 32% as shown in Table IV, which is about a 12% improvement upon the Guellil-Adams model.[9] For comparison, Table IV also gives the forces predicted by several other generated Ta potentials based on parameters taken from the literature. The improved Finnis-Sinclair potential[14] also yielded very good forces although it predicts incorrect interplanar distances for the (100) surface (see below). The qEAM potential[11] gives an overall error in the forces of 133%, and it only reproduces the forces for the cluster better than the Guellil-Adams potential,[9] being worse for the other structures. The MEAM potential also shows large errors (176%) in predicting forces, especially for the liquid-Ta structure; it also fails to reproduce forces for the other high-temperature and defect structures. The relatively large error in forces obtained for the qEAM and MEAM potentials suggests that these potentials may need to include more data in their input database that is commensurate with their relatively large number of function parameters. However, although the present potential does a good job of reproducing DFT forces relative to the other potentials, the absolute value of error in fitting (32%) is still large in comparison to potentials generated for Al (~18%),[17] Mg (~18%),[18] Al-Mg (~22%),[19] Al-Cu (~21%),[20] and Al-Pb (~20%).[21] This is presumably because the simple EAM does not contain an angular term, so it is limited in its ability to describe bonding between partially filled *d* orbitals. As pointed out by other investigators, the partially filled *d* orbitals make the outer shell of the electron density deviate from spherical symmetry, and the host electron density deviates from the superposition of atomic electron density for bcc metals.[42,43] It can also be seen from Table IV that the fit of forces for bulk structures is better than that for other structures such as clusters, surfaces, and liquids. This is further confirmed by our fitting the potential only to forces for bulk crystal structures at temperature below 2500 K where we find the force errors to be much smaller (about 20%), while maintaining good agreement with the other bulk properties. Therefore, it appears that the simple EAM model is reasonably correct for describing bulk properties of bcc metals at moderate temperatures. Although including an angular term could improve transferability, it would greatly increase computational cost. Here we have shown that by performing a careful fit, a Ta potential with reasonably good transferability is possible, even within the simple EAM formalism.

We performed some preliminary tests on the fitted potential. We first examined the relative stability of the bcc, fcc, and β-Ta phases by calculating their respective cohesive energies (see Table V). We find that the bcc phase is most stable, having the greatest cohesive energy (absolute value), the fcc phase is least stable, and the β phase falls in between. This is consistent with experiment since the bcc structure is found to be the stable structure at room temperature; β-Ta has $P4_2/mnm$ symmetry and appears as a metastable structure in epitaxial growth of Ta films for Cu metallization.[5] These calculations are also in agreement with our DFT calculations in terms of the relative stability of these structures.

For our next test, we calculated the relaxed vacancy migration energy and formation energies (Table VI). The migration energy (1.24 eV) was calculated with a conjugate gradient energy minimization since an atom was moved from one site into the neighboring vacancy site using a simple drag method. The relaxed vacancy formation energy (2.76 eV) is in good agreement with experimental data (2.8 ± 0.6 eV).[44] Likewise the sum of vacancy formation energy and migration energies (4.00 eV) is in good agreement with

TABLE III. Fitted results for experimental and calculated data by DFT. The data for error (%) by the Guellil-Adams potential are calculated from Ref. 9.

Parameters	Data calculated by this potential	Experimental data and calculated data by DFT	Error (%)	Error (%) by Guellil-Adams potential
Lattice constant (Å)	3.3026	3.3026		
Cohesive energy (eV)	−8.089	−8.089		
Bulk modulus (Gpa)	179.2	194.2	8	27
C_{11}-C_{12} (Gpa)	103.9	108.2	4	3
C_{44} (Gpa)	86.5	87.4	1	4
Unrelaxed vacancy Formation energy (eV)	2.94	2.95	0.3	1
FCC cohesive energy (eV)	−7.94	−7.81	2	1

TABLE IV. Fit of forces. Data for error of prediction by the Guellil-Adams potential are calculated from Ref. 9. Data for the improved Finnis-Sinclair potential are calculated using Ref. 14. Data for the qEAM are calculated from Ref. 11. Data for the MEAM are calculated from Ref. 10.

Structure number	Structure name	Error of fit	Error of prediction by Guellil-Adams potential	Improved Finnis-Sinclair potential	qEAM	MEAM
1	BCC Ta, ~ 2500 K	24%	32%	34%	111%	100%
2	BCC Ta, ~500 K	26%	28%	27%	152%	82%
3	β-Ta, ~1000 K	24%	32%	28%	109%	113%
4	β-Ta, ~2000 K	23%	32%	33%	118%	124%
5	β-Ta, surface at 500 K with adatoms	41%	57%	37%	160%	170%
6	β-Ta surface at 500 K with more adatoms	37%	55%	38%	135%	216%
7	BCC Ta, stacking fault	58%	41%	57%	173%	254%
8	BCC Ta, ~1500 K, one vacancy	35%	52%	52%	174%	122%
9	10 Ta, atom cluster, ~500 K	42%	91%	59%	79%	114%
10	liquid Ta, ~4500 K	45%	61%	50%	150%	714%
11	BCC Ta, one interstitial, 1500 K	26%	39%	35%	115%	111%
Average		32%	44%	39%	133%	176%

TABLE V. Difference in cohesive energies for different structures predicted by the potential with respect to that of BCC Ta.

Structure	Predicted cohesive energy with respect to BCC Ta (eV)	Calculated cohesive energy by DFT with respect to BCC Ta (eV)
BCC	0.000	0.000
FCC	0.137	0.277
β-Ta (30 atoms/cell)	0.076	0.024

TABLE VI. Comparison of vacancy formation, migration, and self-diffusion data. Data for the improved Finnis-Sinclair potential are calculated from Ref. 14. Data for the Guellil-Adams potential are calculated from Ref. 9. Data for the qEAM are from the potential used in Ref. 11. Data for the MEAM are from Ref. 10. DFT-LDA data are from Ref. 47. Data for experiment are from Refs. 44–46.

	Vacancy migration energy (eV)	Vacancy formation energy (eV) (relaxed)	Vacancy diffusion activation energy (eV)
This work	1.24	2.76	4.00
Improved Finnis-Sinclair	1.22	2.87	4.09
Guellil-Adams	1.15	2.76	3.91
qEAM	1.09	2.94	4.03
MEAM	0.76	2.95	3.71
DFT-LDA data	0.8	3.0	3.8
Experiment		2.8 ± 0.6	3.8 ± 0.3

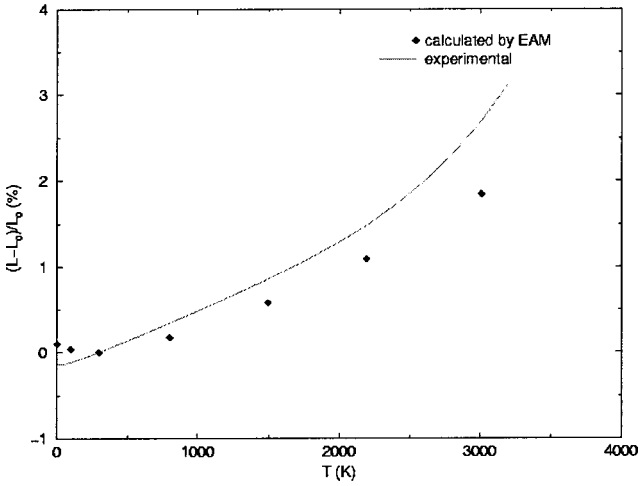

FIG. 4. Comparison of predicted data and experimental data for the linear thermal-expansion coefficient. The solid line represents experimental data and the diamond points are the calculated data with our fitted potential.

the experimental activation energy for diffusion of 3.8 ± 0.3 eV.[45,46] These data are also comparable to data calculated using the improved Finnis-Sinclair[14] potential, Guellil-Adams potential,[9] and the qEAM potential.[11] However, the relaxed vacancy formation energies by these empirical potentials are lower than DFT data[47] whereas the vacancy migration energy is higher than DFT data.[47] The reported data[10] calculated using the MEAM potential agree well with the DFT data.[47] We also calculated the vacancy formation volume with a supercell of 432 atoms, and found a contraction of 34% of equilibrium atomic volume (V_0), which gives a vacancy formation volume of 66% V_0. This is in good agreement with $(60\pm 10)\%$ V_0 predicted by DFT.[47]

The calculated linear thermal expansion curve is shown in Fig. 4. The calculation was done by molecular-dynamics simulations with the present potential, to determine the lattice constants that correspond to zero pressure at different temperatures relative to 298 K. The calculated data are in reasonable agreement with the experimental data[48] with discrepancy between the calculation and experimental data increasing with temperature up to a maximum error of ~30%. At very low temperatures, the potential has a small negative thermal expansion, which is incorrect.

TABLE VII. Comparisons of relaxed surface energies. Data for the Guellil-Adams potential, improved Finnis-Sinclair potential, Baskes' MEAM, and the qEAM are calculated from Refs. 9, 14, 10, and 11, respectively. Data for 0-K estimates are from Ref. 9. DFT-LDA data are from Ref. 50.

	(100) surface (J/m^2)	(110) surface (J/m^2)
This work	2.03	1.77
Guellil-Adams	1.99	1.80
Improved Finnis-Sinclair	2.33	1.98
Baskes' MEAM	3.04	2.78
QEAM	1.75	1.47
DFT-LDA data	2.82–2.97	2.58
0-K estimates[a]	2.87	2.02

[a]Estimated based on Tyson's "population density factor."

TABLE VIII. Distances between the surface layers for (100) and (110) planes. Data for the Guellil-Adams EAM potential, the improved Finnis-Sinclair potential, and the qEAM are calculated from Refs. 9, 14, and 11, respectively. Data for experiment are from Ref. 9. DFT-LDA data are from Ref. 50.

	(100) relaxation, %		(110) relaxation, %	
Data source	Δ^{12a}	Δ^{23b}	Δ^{12a}	Δ^{23b}
This work	−2.3	+0.10	−0.99	+0.05
Guellil-Adams EAM	+2.4	−1.2	−1.0	+0.03
Improved Finnis-Sinclair	−3.5	−1.0	−2.8	+0.2
qEAM	−1.1	−0.5	−0.08	+0.007
DFT-LDA	−12	+4	−2	3
Experiment	−11	+1		

[a]Distance between the first and second layers.
[b]Distance between the second and third layers.

Moving next to surface properties, the relaxed surface energy was calculated to be 2.03 J/m^2 for (100) and 1.77 J/m^2 for (110). The average experimental surface energy extrapolated to zero Kelvin is about 2.78–2.90 J/m^2.[10,49] Previous DFT data[50] for (100) and (110) surfaces are listed at 2.82–2.97 and 2.58 J/m^2 in Table VII. As shown in Table VII, the EAM surface energies are about 12%–29% lower than the estimates using Tyson's population density factor[9] based on extrapolated experimental data, which is typical for EAM potentials. The MEAM potential gives a value that is higher than the estimate for the (100) surface.[10] The qEAM gives lower surface energy values for both (100) and (110) surfaces. The DFT data[50] agree well with Tyson's estimate for (100) but are higher than Tyson's estimate for (110).

The reconstruction of the (100) surface of W was observed by Altman, Estrup, and Robinson.[51] Xu and Adams[52] pointed out that the reconstruction of surfaces of W and Mo was presumably ascribed to the angular-dependent forces. Our Ta potential does not produce a surface reconstruction on the Ta (100) surface. Table VIII shows the two near-surface interplanar distances for (100) and (110) planes, which are in qualitative agreement with experiment data and DFT calculations.[50] The improved Finnis-Sinclair potential[14] and the qEAM[11] potential predict a contracted second interplanar distance at the (100) surface. The Guellil-Adams potential[9] predicts an expanded first interplanar distance at the (100) surface. All three predictions contradict experimental observations and DFT calculations.[9]

Including angular terms into the Ta potentials in practice greatly increases the computational cost. Xu and Adams[52] added the third and fourth moments in their EAM potentials for W, Mo, and V, which resulted in improved descriptions of surfaces properties but at the cost of a 100-fold increase in computational time.

Baskes modified the EAM by introducing an angular term into the functional form[53] to reflect the angular dependence present in the electron density of the same materials. The

surface energies by such a MEAM Ta potential is closer to experimental data than most EAM potentials. However, our test of the potential shows that the MEAM Ta potential shows relatively large errors in forces with respect to DFT forces. Zhang *et al.* introduced a different term, a modified energy term, into the total-energy expression of the MEAM and obtained good results for reproducing experimental data for Ta vacancy formation energy and migration energy.[43] This MEAM potential is also in analytical form. It would be useful to further test these potentials in more detail.

IV. CONCLUSIONS

A new EAM potential for Ta has been created by fitting to a variety of experimental data, equation of state data, and first-principles data including hundreds of DFT forces from a variety of structures including clusters, surfaces, interstitials, vacancies, liquids, and stacking faults as well as bulk crystal structures at different temperatures. The newly fitted potential has a better overall fit to DFT forces than the previous Guellil-Adams potential, but the improved Finnis-Sinclair potential is of comparable accuracy. In contrast, our tests on the qEAM and MEAM potentials show relatively poor agreement with our DFT force database.

Further testing of the potential revealed good qualitative agreement with that of DFT calculations in predicting the correct stable structure for Ta as well as for the metastable structure β-Ta. The potential also predicts reasonable vacancy formation and migration energies. The calculated thermal expansion is generally lower than the experimental value with the largest error on the order of ~30%. The average surface energies for (100) and (110) planes are about 12%–30% lower than DFT data and Tyson's estimates based on experiments. The calculated interplanar displacement for the (100) surface is also in qualitative agreement with both experimental observations and DFT data. We recommend that other researchers consider these Ta potentials or the revised Finnis-Sinclair Ta potential over other current potentials due to their good description of DFT forces and low computational cost.

ACKNOWLEDGMENTS

We thank Furio Ercolessi for initial development of the fitting code. The current version of the fitting code is available at http://www.public.asu.edu/~liyh29/; this fitted Ta potential and many others are also available at the website. We thank M. I. Baskes for sharing his MEAM code with us and useful discussions about the MEAM. We also thank William A. Goddard III's group for sending us their preprint paper on qEAM potentials. We thank David Richards for his discussion about the fitting code. We also thank S. F. Foiles, M. I. Baskes and M. S. Daw for use of the DYNAMO code and Jun Zhong for useful discussions. This work is supported by the National Science Foundation through Grant No. ASC97-40300, via a subcontract from the National Center for Supercomputing Applications (NCSA).

[1] D. Denning, G. Braeckelmann, J. Zhang, B. Fiordalice, and R. Venkatramen, in *Digest of Technical Papers, 1998 Symposium on VLSI Technology*, edited by The Institute of electrical and Electronics Engineers (IEEE, New York, 1998), p. 22.

[2] T. Hara, T. Tomisawa, T. Kurosu, T. K. Doy, and K. Sakai, Electrochem. Solid-State Lett. **2**, 339 (1999).

[3] Y. T. Hao, S. C. Sun, and J. W. Shui, J. Electrochem. Soc. **147**, 2766 (2000).

[4] K. Weiss, S. Riedel, S. E. Schulz, M. Schwerd, H. Helneder, H. Wendt, and T. Gessner, Microelectron. Eng. **50**, 433 (2000).

[5] K-W. Kwon, C. Ryu, R. Sinclair, and S. S. Wong, Appl. Phys. Lett. **71**, 3069 (1997).

[6] S. S. Wong, C. Ryu, H. Lee, A. L. S. Loke, K. W. Kwon, S. Bhattacharya, R. Eaton, R. Faust, B. Mikkola, J. Mucha, and J. Ormando, in *Proceedings of the IEEE 1998 International Interconnect Technology Conference*, edited by The Institute of Electrical and Electronics Engineers (IEEE, New York, 1998), pp. 107–109.

[7] M. W. Finnis and J. E. Sinclair, Philos. Mag. A **50**, 45 (1984).

[8] R. A. Johnson and D. J. Oh, J. Mater. Res. **4**, 1195 (1989).

[9] A. M. Guellil and J. B. Adams, J. Mater. Res. **7**, 639 (1992).

[10] B-J. Lee, M. I. Baskes, H. Kim, and Y. K. Cho, Phys. Rev. B **64**, 184102 (2001).

[11] G. Wang, A. Strachan, T. Cagin, and W. A. Goddard III, Mater. Sci. Eng., A **309-310**, 133 (2001).

[12] M. Mrovec, V. Vitek, M. D. Nguyen, D. G. Pettifor, L. G. Wang, and M. Sob, in *Multiscale Phenomena in Materials—Experiments and Modeling*, edited by D. H. Lassila, I. M. Robertson, R. Phillips, and B. Devinere, Mater. Res. Soc. Symp. Proc. No. **578** (Materials Research Society, Pittsburgh 2000), p. 199.

[13] J. A. Moriarty, J. F. Belak, R. E. Rudd, P. Söderlind, F. H. Streitz, and L. H. Yang, J. Phys.: Condens. Matter **14**, 2825 (2002).

[14] G. J. Ackland and M. W. Finnis, Philos. Mag. A **54**, 301 (1986).

[15] R. Rebonato, D. O. Welch, R. D. Hatcher, and J. C. Bilello, Philos. Mag. A **55**, 655 (1987).

[16] P. Vinet, J. Ferrante, J. R. Smith, and J. H. Rose, J. Phys. C **19**, L467 (1986); P. Vinet, J. H. Rose, J. Ferrante, and J. R. Smith, J. Phys.: Condens. Matter **1**, 1941 (1989).

[17] F. Ercolessi and J. B. Adams, Europhys. Lett. **26**, 583 (1994).

[18] X.-Y. Liu, J. B. Adams, F. Ercolessi, and J. A. Moriarty, Modell. Simul. Mater. Sci. Eng. **4**, 293 (1996).

[19] X.-Y. Liu, P. P. Ohotnicky, J. B. Adams, C. L. Rohrer, and R. W. Hyland, Jr., Surf. Sci. **373**, 357 (1997).

[20] X.-Y. Liu, Wei Xu, S. M. Foiles, and J. B. Adams, Appl. Phys. Lett. **72**, 1578 (1998).

[21] A. Landa, P. Wynblatt, D. J. Siegel, J. B. Adams, O. N. Mryasov, and X.-Y. Liu, Acta Mater. **48**, 1753 (2000).

[22] M. S. Daw and M. I. Baskes, Phys. Rev. B **29**, 6443 (1984).

[23] P. Hohenberg and W. Kohn, Phys. Rev. B **136**, B864 (1964).

[24] W. Kohn and L. J. Sham, Phys. Rev. A **140**, A1133 (1965).

[25] J. Kohanoff and J. P. Hansen, Phys. Rev. E **54**, 768 (1996).

[26] V. B. Shenoy, R. Miller, E. B. Tadmor, R. Phillips, and M. Ortiz, Phys. Rev. Lett. **80**, 742 (1998).
[27] D. Y. Sun and X. G. Gong, Phys. Rev. B **57**, 4730 (1998).
[28] O. Gülseren, F. Ercolessi, and E. Tosatti, Phys. Rev. Lett. **80**, 3775 (1998).
[29] W. Fan, Yizhen He, and X. G. Gong, Philos. Mag. A **79**, 1321 (1999).
[30] B. Edwards, N. W. Ashcroft, and T. Lenosky, Europhys. Lett. **34**, 519 (1996).
[31] T. J. Lenosky, J. D. Kress, I. Kwon, A. F. Voter, B. Edwards, D. F. Richards, S. Yang, and J. B. Adams, Phys. Rev. B **55**, 1528 (1997).
[32] U. Hansen, P. Vogl, and V. Fiorentini, Phys. Rev. B **59**, R7856 (1999).
[33] U. Hansen, P. Vogl, and V. Fiorentini, Phys. Rev. B **60**, 5055 (1999).
[34] T. J. Lenosky, B. Sadigh, E. Alonso, V. V. Bulatov, T. Diaz-de-la-Rubia, J. Kim, A. F. Voter, and J. D. Kress, Modell. Simul. Mater. Sci. Eng. **8**, 825 (2000).
[35] Y. Mishin, D. Farkas, M. J. Mehl, and D. A. Papaconstantopoulos, Phys. Rev. B **59**, 3393 (1999).
[36] G. Kresse and J. Furthmuller, Phys. Rev. B **54**, 11 169 (1996).
[37] G. Kresse and D. Joubert, Phys. Rev. B **59**, 1758 (1999).
[38] P. E. Blochl, Phys. Rev. B **50**, 17 953 (1994).
[39] J. P. Perdew, J. A. Chevary, S. H. Vosko, K. A. Jackson, M. R. Pederson, D. J. Singh, and C. Fiolhais, Phys. Rev. B **46**, 6671 (1992).
[40] H. J. Monkhorst and J. D. Pack, Phys. Rev. B **13**, 5188 (1976).
[41] J. H. Rose, J. R. Smith, F. Guinea, and J. Ferrante, Phys. Rev. B **29**, 2963 (1984).
[42] J. B. Adams and S. M. Foiles, Phys. Rev. B **41**, 3316 (1990).
[43] B. Zhang, Y. Ouyang, S. Liao, and Z. Jin, Physica B **262**, 218 (1999).
[44] K. Maier, M. Peo, B. Saile, H. E. Schaefer, and A. Seeger, Philos. Mag. A **40**, 701 (1979).
[45] D. Weiler, K. Maier, and H. Meher, in *Diffusion in Metals and Alloys*, edited by F. J. Kedves and D. L. Beke (Trans. Tech. Publ., Aedermannsdorf, Switzerland, 1983), p. 342.
[46] R. E. Pawel and T. S. Lundy, J. Phys. Chem. Solids **26**, 937 (1965).
[47] A. Satta, F. Willaime, and S. de Gironcoli, Phys. Rev. B **60**, 7001 (1999).
[48] Y. S. Touloukian, R. K. Kimrby, R. E. Taylor, and P. D. Desai, *Thermophysical properties of Matter, Thermal expansion, Metallic Elements and Alloys* (Plenum, New York, 1970), Vol. 12, p. 361.
[49] W. R. Tyson, J. Appl. Phys. **47**, 459 (1976).
[50] C. J. Wu, L. H. Yang, J. E. Klepeis, and C. Mailhiot, Phys. Rev. B **52**, 11 784 (1995).
[51] M. S. Altman, P. J. Estrup, and I. K. Robinson, Phys. Rev. B **38**, 5211 (1988).
[52] W. Xu and James B. Adams, Surf. Sci. **301**, 371 (1994).
[53] M. I. Baskes, Phys. Rev. B **46**, 2727 (1992).